Unveiling the phenol direct carboxylation reaction mechanism at ZrO2 surface

Kaihua Zhang, Changru Ma, Sebastien Paul, Jeremie Zaffran

Molecular Catalysis 569 (2024) 114606

Contents lists available at ScienceDirect

Molecular Catalysis

journal homepage: www.journals.elsevier.com/molecular-catalysis

Unveiling the phenol direct carboxylation reaction mechanism at ZrO2 surface

Kaihua Zhang [a], Changru Ma [a], Sebastien Paul [b,1], Jeremie Zaffran [a,*,2]

[a] Eco-Efficient Products and Processes Laboratory (E2P2L),IRL 3464 CNRS-Syensqo, 3966 Jin Du Road, Xin Zhuang Ind. Zone, 201108 Shanghai, China
[b] Univ. Lille, CNRS, Centrale Lille, Univ. Artois, UMR 8181 - UCCS - Unité de Catalyse et Chimie du Solide, F-59000 Lille, France

ARTICLE INFO

Keywords:
CO_2 valorization
aromatics carboxylation
C-H activation
heterogeneous catalysis
density functional theory (DFT) computation

ABSTRACT

In the present context of environmental concerns, sustainable solutions must be proposed to dispose of waste CO_2, a well-known greenhouse gas. Among the various emerging projects, upgrading CO_2 molecule into high-value added chemicals appears to be very promising. More particularly, the carboxylation of aromatic compounds to (di-) acid aromatic monomers is of great interest for the high performance polymer industry. Focusing on the direct phenol carboxylation to *para*-hydroxybenzoic acid as a model reaction, the reactivity of ZrO_2 was investigated in this paper, this material being recently reported in various experimental works for its catalytic efficiency. For the first time, we established the phenol carboxylation mechanism at the surface of a metal oxide material, showing that the reaction can only proceed through an Eley-Rideal mechanism. In this mechanism, CO_2 is strongly chemisorbed at the surface, whereas phenol is physisorbed close to the CO_2 adsorbate. Besides, while the monoclinic and the tetragonal phases often coexist in ZrO_2 particles, we demonstrated that only the monoclinic geometry exhibits a substantial activity. However, the selectivity remains a major challenge, the *ortho*- isomer being the most abundant product, as in the original Kolbe-Schmitt method. While most of the processes generally reported in literature for the direct carboxylation of phenol are achieved in liquid media, a very few theoretical knowledge is available to describe such a process at solid surfaces. Therefore, we expect the present manuscript to be a pioneer work, aiming at providing a better understanding of metal oxide surface reactivity, paving the road to the rational design of efficient solid catalysts for aromatics carboxylation reactions.

Introduction

In the current context of environmental concern, various methods have been proposed to dispose of carbon dioxide (CO_2) waste and to valorize biomass [1,2]. Especially, bio-derived aromatic compounds can be carboxylated in order to be upgraded into monomers of interest to manufacture high performance polymers [3,4]. Such a strategy could limit resorting to fossil resources in the plastic materials industry, and would thus contribute to improve the environmental quality [5,6]. However, the direct carboxylation of aromatics faces major challenges, mostly related to the high stability of the CO_2 molecule [7,8] and to the difficulty of aromatics' C-H bond activation [9,10]. The catalyst rational design is thus of primary importance for this project, and it can be achieved combining experiment and computational chemistry tools [11,12].

Among the various aromatic compounds of potential interest, a special attention shall be paid to phenol, since it can be derived from biomass [13]. While different methods are commonly used to produce such a molecule, recent bio-based strategies involving the lignocellulose decomposition have emerged [14]. Hence, the direct phenol carboxylation starting from waste CO_2 may be envisaged as an ambitious green process, leading to several aromatic carboxylic acids relevant to the chemical industry [15]. However, such a one-pot synthesis is very challenging, mostly in reason of the high stability of the CO_2 molecule. Indeed, CO_2 activation generally requires high temperature and pressure, including harsh conditions with strong bases and toxic halide precursors [16]. Therefore, in the current context of societal environment concerns, developing an eco-friendly process for such a reaction is a necessity.

In a very recent study, Pandey et al. describe a novel synthesis

* Corresponding author.
E-mail address: jeremie.zaffran@cnrs.fr (J. Zaffran).
[1] ORCID: 0000-0001-9877-9902.
[2] ORCID: 0000-0003-3176-6140.

https://doi.org/10.1016/j.mcat.2024.114606
Received 9 July 2024; Received in revised form 5 October 2024; Accepted 6 October 2024
Available online 13 October 2024

method for the conversion of phenol and CO_2 into hydroxybenzoic acid (HBZA), catalyzed by Cu doped ZrO_2 particles [17]. Unlike the well-known Kolbe-Schmitt process, operating in liquid phase with hydroxide anions as homogeneous catalyst [18], their work does not require any strong base or toxic salt. While the *para* carboxylation is expected for various applications in the polymer industry [19], the *ortho* position appears to be generally more favorable, as resulting from the Kolbe-Schmitt reaction [16-18]. In the framework of heterogeneous catalysis, such a selectivity issue can be addressed by tuning the chemical properties of the catalyst surface, including the vacancy amount, the doping ratio and the dopant nature [20-22]. The aim of this paper is to use density functional theory (DFT) computation in order to understand ZrO_2 reactivity, and the various parameters involved in its activity and selectivity. Further, such a knowledge will be of first importance for the rational design of metal oxide catalysts, with an appropriate doping ratio.

Considering pure ZrO_2 as a reference model catalyst, we investigated the direct carboxylation of phenol into HBZA. Although the major part of this manuscript is devoted to the reaction mechanism identification, we first discussed the O vacancy effect on the surface reactivity. While the first two sections of this manuscript are related to monoclinic ZrO_2, we also investigated in the last part the tetragonal phase reactivity. Indeed, both geometries share common borders in their phase diagram [23], and thus they are often found mixed together in ZrO_2 nanoparticles [24,25].

Methods and materials

Computational details

This computational work was achieved with the VASP 5.4 package [26], using the Perdew−Burke−Ernzerhof (PBE) exchange−correlation (XC) functional [27]. All our calculations were performed in the periodic density functional theory (DFT) framework. Considering that several studies dealing with metal oxide materials include the Hubbard correction [28], we carried out some additional tests comparing simple DFT and DFT+U, both methods resulting in similar trends regarding ZrO_2 reactivity (see section 1 in the Supplementary Information, SI). In the Monkhorst−Pack scheme [29], Gamma centered k-meshes of 25 × 25 × 25 and of 5 × 5 × 1 points were set for bulk and slab computation, respectively. The projected augmented waves (PAW) formalism [30] was used to model the core-electron interaction, with a cutoff energy of 400 eV. We considered an energy convergence criterion of 10^{-6} eV for electronic optimization, and a force convergence criterion of 0.05 eV/ Å for ionic relaxation. All those parameters lead reaction and activation energies to be converged in the range of ~0.05 eV. The Henkelman tools were used for the Bader charge analysis [31-33] and for the transition state search, achieved by the means of the nudged elastic band (NEB) [34,35] and the dimer methods [36] and then confirmed by frequency calculations revealing a single imaginary vibration mode. No zero point energy (ZPE) or entropy corrections were included in our results. Such an approximation is acceptable since all our energetics computations only deal with adsorbed intermediates, and are not referred to any gas phase species, hence limiting the potential errors related to the entropic effect. Finally, let us highlight that for each elementary step, reaction energy and activation barrier were assessed considering all the intermediate species adsorbed at different slabs, and not co-adsorbed together. Concerning the Eley-Rideal mechanism, the energetic reference is the reactant with CO_2 adsorbed in its most stable configuration, and phenol in gas phase

Material and surface structure

We focused on two stable ZrO_2 geometries in the usual range of temperatures and pressures, namely the monoclinic and the tetragonal phases (respectively denoted m-ZrO_2 and t-ZrO_2, further) [37]. We first optimized the two bulk structures allowing the lattice parameters to relax. Regarding m-ZrO_2, we reached a=5.14 Å, b=5.22 Å and c=5.32 Å for the lattice constants, and α=γ=90° and β=90.42° for the angles. Concerning t-ZrO_2, we reached a=b=3.59 Å and c=5.21 Å for the lattice constants, and α=β=γ=90° for the angles. All those computed values are in fair agreement with experimental reported data, attesting the validity of our calculation method [38,39]. Then, we created slabs, cleaving each of the bulks according to the (111) and the (101) facets for the monoclinic and the tetragonal phases, respectively. Such surfaces are already reported in literature to be among the most abundant facets in m-ZrO_2 and t-ZrO_2 nanoparticles [40,41]. The size of the cell was set to $p(1 \times 1)$ for m-ZrO_2 (111) and to $p(1 \times 2)$ for the t-ZrO_2 (101), hence reaching a similar coverage at both surfaces. Let us mention increasing the cell dimensions does not induce any major change in reaction energy or kinetic barrier assessment (see section 2 in the SI). Each of them includes four metal oxide atomic layers, none of them being constrained during the computational relaxation process, resulting in symmetric slab models. In addition, a fixed 15 Å vacuum layer was set above the surface to avoid virtual interaction between the periodic images in the z direction. Regarding reactivity calculation, an extensive configuration pre-screening was achieved for every reaction intermediate and transition state (IS and TS, respectively), and only the most stable adsorption mode was selected for each species. Also, while various O vacancy locations were tested at the bare m- and t-ZrO2 slabs, only the most stable surface was finally retained for each phase to study the catalyst reactivity.

Results and discussion

In this section, we will demonstrate CO_2 activation is made possible owing to the presence of O vacancies at the metal oxide catalyst surface, enabling a direct interaction between the C and the Zr atoms. The considerable adsorption strength of CO_2 compared to phenol and other intermediates suggests an Eley-Rideal (ER) single step mechanism, rather than a Langmuir-Hinshelwood (LH) multistep process. Finally, while both the ZrO_2 monoclinic and tetragonal phases are often reported coexisting and difficult to dissociate, we showed only the monoclinic phase is active in the phenol direct carboxylation reaction.

On the role of surface O vacancies

Since O vacancies are very common on ZrO_2 surface [42], we addressed the reactivity of the perfect and defected m-ZrO_2 surfaces. In both situations, we performed an extensive screening of the phenol and CO_2 configurational space (see SI, section 5A). Concerning phenol, we identified two major modes of adsorption at the perfect surface, with the aromatic ring either orthogonal or parallel to the ZrO_2 plan. The molecule is either stabilized by chemisorption through Zr-O binding or by physisorption via H bonds between the phenol OH group and some surface O atoms. The most stable configuration results in a weak binding energy of -0.37 eV. Regarding the O defected surface, C-C *pi* interactions with vacant Zr atoms are also observed, hence increasing phenol adsorption strength with an adsorption energy of -1.68 eV, and constraining the molecule to adopt a adsorption mode parallel to the surface. Notably, although some metal sites are vacant following the surface O removal, it was not possible to stabilize any chemical bonding between the phenol OH group and the defected Zr atoms. Interestingly, considering the energy distribution of the various configurations, and especially the bottom range including the most stable and adsorption modes, we can see that most of the structures present very similar energies, with slight discrepancies on the order of 0.10-0.20 eV both for the perfect and the defected surface. Such an observation attests the facile diffusion of phenol, especially at the perfect surface, and the difficulty to activate the aromatic ring C-H bond at ZrO_2. The most stable phenol configurations are displayed below in the top panel of Fig. 1.

Regarding CO_2, the molecule is very stable in the gas phase, and thus

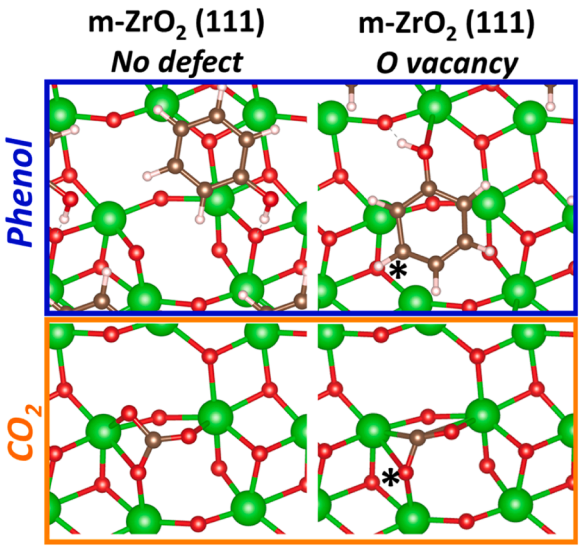

Fig. 1. Top view of the most stable configurations of phenol (top panel) and CO2 (bottom panel) adsorbates at the surface with no defects (left side) and with O vacancies (right side). For clarity reasons, only the ZrO2 topmost layer unit cell of the slab is represented. The "*" sign denotes the O vacancy location. Ball & stick color code: green, Zr; brown, C; red, O; pinkish, H.

is especially laborious to adsorb. Among the few configurations we identified at the perfect surface, the most stable exhibits a distorted CO_2 molecule, where its two O are connected to two distinct Zr atoms, and its C is linked with a surface O atom, resulting in a adsorption energy of -1.05 eV. However, the presence of an O vacancy at the surface brings to a tremendous stabilization of CO_2 adsorbate, significantly increasing the Zr-C bond ionicity (see the Bader charge analysis in the SI, section 3) and decreasing the adsorption energy up to -3.26 eV. In the most stable adsorption mode, the two defected metallic sites establish a strong linkage with the adsorbate C and O atoms, hence bending the molecule skeleton and activating CO_2 species. Therefore, O vacancies play a crucial role in metal oxide reactivity, especially for carboxylation reactions, CO_2 adsorption being the driving force of the reaction. The most stable CO_2 configurations are displayed below in the bottom panel of Fig. 1.

The Langmuir-Hinshelwood vs. Eley-Rideal mechanism

Now we established the necessity of O vacancies to initiate the reaction, we will investigate the phenol carboxylation mechanism through two different widely known processes in heterogeneous catalysis, only focusing on the defected ZrO_2 surface: the Langmuir-Hinshelwood (LH) [43] and the Eley-Rideal (ER) [44] mechanisms. We will first consider the carboxylation attack at the *para-* position, before envisaging the *meta-* and *ortho-* possibilities. All the IS and TS structure coordinates used for the various reaction pathways are reported in the SI, section 6.

The Langmuir-Hinshelwood mechanism

The LH mechanism is very common in heterogeneous catalysis. It generally consists in a multi-step process, where all the reacting intermediates are chemisorbed at the surface. In the present situation, the phenol carboxylation reaction can be split in three major steps (see Fig. 2). First, an aromatic ring C-H bond is broken in phenol reactant, leading to an aryl intermediate. Second, the radical C atom is coupled with an adsorbed CO_2 molecule, resulting in hydroxybenzoate (HBZ) species. Finally, the carboxylate group is hydrogenated, giving hydroxybenzoic acid (HBZA), the expected product. As a first general observation, we can see none of the various steps is thermodynamically favored. Indeed, while the first two steps are almost athermic, the last one is highly endothermic with a reaction energy of +1.40 eV. However, the major limitation to the reaction arises from kinetics, all the steps exhibiting high barriers. Especially, a tremendous activation energy of 3.52 eV is computed for C-C coupling, appearing to be the determining reaction step. Such barriers are clearly insurmountable, the highest values usually reported in heterogeneous catalysis barely exceeding 1.5-2.0 eV. The main difficulty of the LH mechanism relies on the stabilization of the aryl intermediate. Indeed, while it can be immobilized at the surface through a strong C-Zr binding following the first dehydrogenation step, the radical has to partially dissociate in order to couple with CO_2 at the next step, hence resulting in a highly unstable TS. Although we only considered here the "direct" carboxylation route proceeding through a coupling between the aryl and CO_2 species, similar conclusions were achieved when dealing with the "formic" carboxylation route involving a coupling between the aryl radical and COOH intermediate (see details in the SI, section 4). Therefore, the LH mechanism must be excluded at ZrO_2 surface for the phenol carboxylation, and another reaction route should be proposed.

The Eley-Rideal mechanism

The ER mechanism is not straightforward in heterogeneous catalysis,

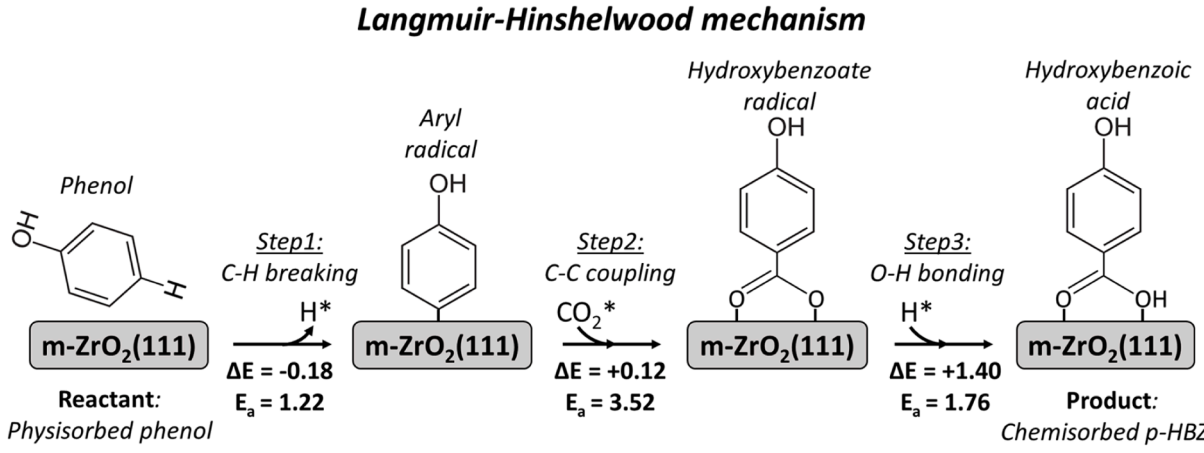

Fig. 2. Langmuir-Hinshelwood mechanism illustrative scheme depicting the three major reaction steps, together with their corresponding reaction intermediates adsorbed at ZrO_2 surface. For each step, the computed reaction energies (ΔE) and activation barriers (E_a) are presented (in eV). Regarding H adatom and CO_2 species, the "*" sign indicates the species are chemisorbed and not in gas phase. The ball and stick models, with their coordinates are reported in the SI, section 6, for the different IS and TS structures.

as it requires a strongly chemisorbed species at the surface, weakly interacting with another physisorbed reagent. Such a conformation gives rise to a concerted mechanism, instead of elementary reaction steps as in the previously described LH process. The general process is depicted in Fig. 3 with all the involved surface intermediates and TS. Here, since CO_2 adsorption exhibits a decisive energetic advantage in comparison with phenol, we considered CO_2 chemisorbed at ZrO_2 surface in its most stable configuration, with a phenol molecule physisorbed at the top of it (see the reactant state in Fig. 3). We were able to identify a single TS, simultaneously achieving the aromatic ring C-H scission, the C-C binding between the aryl group and CO_2 and the O-H bond making leading the final carboxylic acid. The interest presented by such a concerted step is to avoid the formation of any unstable radical intermediate, since all the reaction steps are simultaneously achieved. As a consequence, activation energies dramatically drop from 3.52 eV in the LH mechanism in the C-C coupling step, to 1.62 eV here in the ER model. Although this value is still quite high, such barriers are realistic and only require high temperatures (~400-600 K) to activate undoped ZrO_2 catalyst. That is why metal doping elements are often necessary to reduce activation energies, as Cu in the case of phenol carboxylation [17]. Although it has been rarely observed in surface chemistry, such a concerted mechanism has already been reported at metal oxide catalysts for various reaction involving CO_2 species [45,46].

The selectivity challenge

Now we unveiled the phenol carboxylation mechanism, it is possible to address the selectivity issue. Hence, following a similar ER process, we investigated the formation of three potential products, according to their carboxylation sites, namely *para-*, *meta-* and *ortho-* (leading to *p*-HBZA, *m*-HBZA and *o*-HBZA, respectively). As it can be seen in Fig. 4 (and in Table 1, further), all the species are equally favored by thermodynamics, with exothermic heat of reaction ranging from -0.40 to -0.33 eV for each of them. However, regarding kinetics, *p*- and *m*-HBZA formation requires the highest activation energies, both of them on the order of 1.6-1.7 eV, whereas *o*-HBZA is clearly preferred with a much lower barrier or 1.36 eV. Such an observation can be explained by intramolecular H bonds appearing in *o*-HBZA between the -OH and -COOH groups, hence considerably stabilizing the TS in comparison with the two other products. This computational result highlights the major selectivity challenge of the phenol carboxylation, already

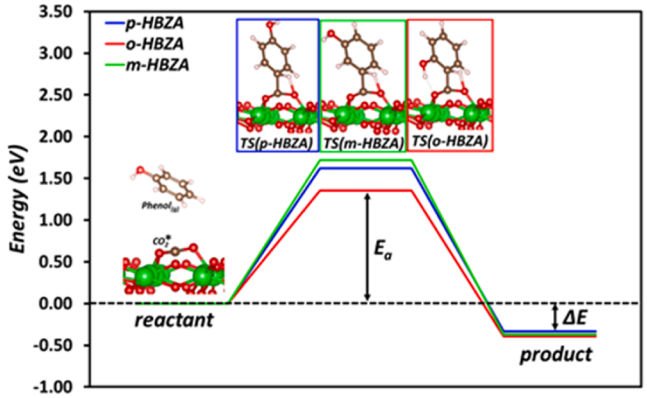

Fig. 4. Eley-Rideal mechanism reaction pathway energy diagram for the phenol direct carboxylation into *p*-, *m*- and *o*-HBZA (plotted in blue, green and red line, respectively). All the energies are referred vs. the most stable CO_2 adsorbate, the phenol molecule being in gas phase. Activation barriers (E_a) and reaction energies (ΔE) are provided in eV for the three reaction products. The three corresponding TS are represented by atomistic models, as well as the reactant state. Ball & stick color code: green, Zr; brown, C; red, O; pinkish, H.

Table 1
Activation barriers (E_a) and reaction energies (ΔE) in eV, related to *p*-, *m*- and *o*-HBZA formation from phenol carboxylation at the monoclinic and the tetragonal ZrO_2 phases (denoted m-ZrO_2 (111) and t-ZrO_2 (101), respectively)

	E_a (eV)		ΔE (eV)	
	m-ZrO_2(111)	*t-ZrO_2(101)*	*m-ZrO_2(111)*	*t-ZrO_2(101)*
p-HBZA	1.62	1.98	-0.33	+0.20
m-HBZA	1.72	2.06	-0.37	+0.22
o-HBZA	1.36	1.61	-0.40	+0.18

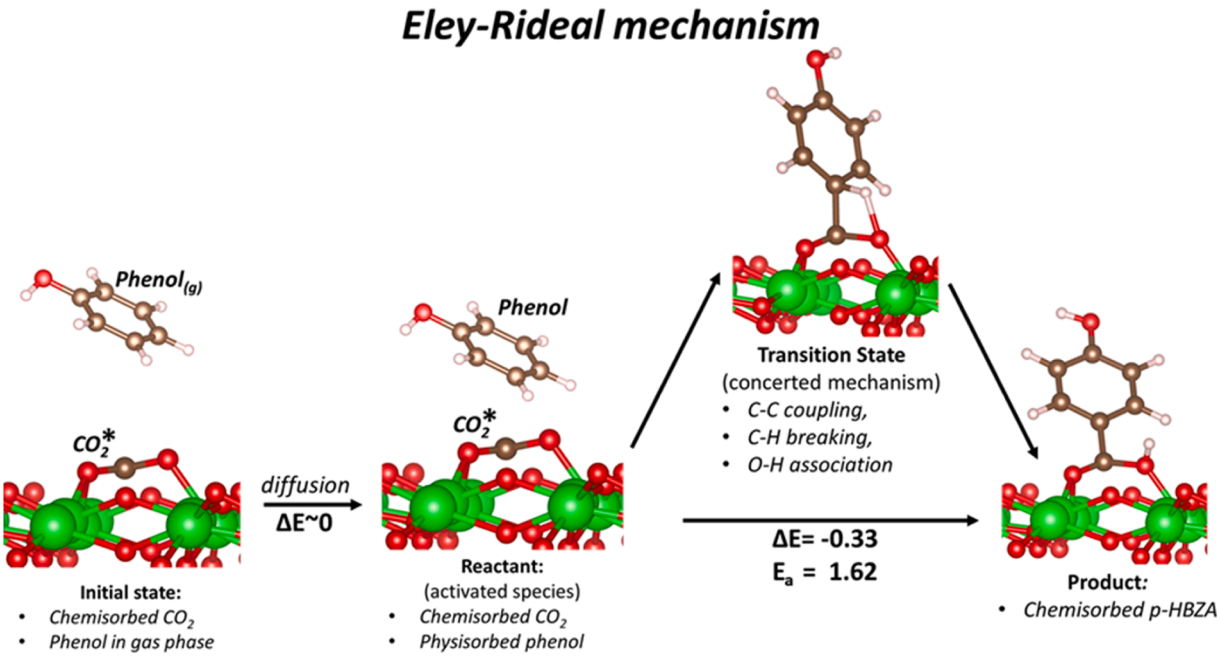

Fig. 3. Eley-Rideal mechanism illustrative scheme depicting the various surface species and reaction steps involved in the phenol direct carboxylation reaction. Activation barrier (E_a) and reaction energies (ΔE) are provided in eV. Although it does not hold a real place in the reaction mechanism itself, we also reported the initial athermic diffusion step, allowing phenol physisorption. When appearing close to the name of a chemical molecule, the "*" sign denotes species chemisorbed at the surface. Ball & stick color code: green, Zr; brown, C; red, O; pinkish, H.

emphasized in the original Kolbe-Schmitt method more than a century ago [18]. Although *o*-HBZA has several applications, mainly in pharmaceuticals and cosmetics, *m*- and more specifically *p*-HBZA have a higher added-value due to their importance in the plastic and materials industry.

The monoclinic vs. tetragonal ZrO2 phase

According to thermodynamics, the ZrO_2 monoclinic phase is the most stable at usual temperature (up to ~700-1000 °C) and pressure (~1-5 bar) working conditions [37,47]. However, considering the existing border in such phase diagrams with the tetragonal phase, especially at high temperature (above ~700 °C), the two phases are difficult to separate from each other and ZrO_2 nanoparticles are often obtained as a mixture of both the monoclinic and the tetragonal phases after calcination [17,24,25]. Therefore, in a reactivity study dealing with metal oxide catalysts, it is crucial to determine the active phase.

In this section, based on the ER mechanism we identified above, we addressed the reactivity of t-ZrO_2 (101) with O vacancies, regarding the phenol carboxylation reaction. The corresponding structures can be found in the SI, section 5B and 6. As observed in Table 1, whatever the carboxylation attack site, the process is endothermic and all the reaction energies are similar, close to +0.20 eV. While such reactions were shown to be highly exothermic previously at m-ZrO2 (111) (see Fig. 4 and Table 1), thermodynamics is not beneficial for the tetragonal phase. Regarding kinetics, the global trends previously observed for selectivity is still preserved, *o*-HBZA product being the less disfavored product compared to *m*- and *p*-HBZA. However, the barriers are generally significantly increased on t-ZrO_2(101) in comparison with m-ZrO_2(111), by an increment of +0.25-0.35 eV according to the product species, even reaching extreme values of ~2.0 eV for *p*- and *m*- HBZA. As a result, the tetragonal phase is clearly inactive in the phenol carboxylation reaction. While some computed kinetic barriers at the monoclinic phase can still be considered as quite high, especially for *m*- and *p*- HBZA, at least thermodynamically all the carboxylation reactions are all strongly exothermic whatever the attack site on the aromatic ring.

Conclusion

As a major achievement of this work, we unveiled the phenol carboxylation mechanism at ZrO_2. We demonstrated the reaction can only proceed through an ER single step process, instead of the LH multistep model generally considered in heterogeneous catalysis. Such a conclusion mainly originates from the aryl radical intermediate instability, stemming from the initial C-H bond scission at the phenol aromatic ring. Therefore, although we established this result at pure ZrO_2, we suggest a similar mechanism can remain valid at various other metal oxide surfaces, for chemical reactions involving C-C coupling between any radical and CO_2 species. The predicted selectivity arising from the ER mechanism is consistent with the original Kolbe-Schmitt phenol carboxylation method, *o*-HBZA being clearly preferred in comparison with *m*- and *p*-HBZA. While similar global trends are observed both at the monoclinic and the tetragonal phases, we highlighted only the monoclinic geometry is active. This latter result is crucial since the two phases are often imbricated into each other in ZrO_2 nanoparticles and difficult to isolate.

The supplementary information contains all the intermediate and transition state structures we considered in this study. The Bader charge analysis in provided in some specific cases. Also, some tests related to DFT+U and to the coverage effect are reported.

CRediT authorship contribution statement

Kaihua Zhang: Investigation, Data curation. **Changru Ma:** Funding acquisition. **Sebastien Paul:** Funding acquisition. **Jeremie Zaffran:** Writing – review & editing, Writing – original draft, Visualization, Validation, Supervision, Resources, Project administration, Methodology, Investigation, Funding acquisition, Formal analysis, Data curation, Conceptualization.

Declaration of competing interest

The authors declare that they have no known competing financial interests or personal relationships that could have appeared to influence the work reported in this paper.

Acknowledgements

We acknowledge the French National Agency of Research (ANR), under grant ANR-21-CHIN-0005-01, for funding this work in the frame of the "PLASTILOOP 2.0" project, in collaboration with University of Lille and in partnership with Syensqo Company.

Supplementary materials

Supplementary material associated with this article can be found, in the online version, at doi:10.1016/j.mcat.2024.114606.

Data availability

data provided in the SI.

References

[1] D. Rodríguez-Padrón, A.R. Puente-Santiago, A.M. Balu, M.J. Muñoz-Batista, R. Luque, Environmental catalysis: present and future, Chem. Cat. Chem. 11 (1) (2019) 18–38.
[2] S. Feng, Y. Geng, H. Liu, H. Li, Targeted intermetallic nanocatalysts for sustainable biomass and CO2 valorization, ACS Catalysis 12 (24) (2022) 14999–15020.
[3] M.G. Zolotukhin1, S. Fomine, L.M. Lazo, M.D.C.G. Hernández, M.T. Guzmán-Gutiérrez, A. Ruiz-Trevino, D. Fritsch, D.C. Cuellas, J.M. Fernandez-G, A novel approach to the synthesis of high performance and functional polymers, High Perform. Polym. 19 (5-6) (2007) 638–648.
[4] P.M. Hergenrother, The use, design, synthesis, and properties of high performance/high temperature polymers: an overview, High Perform. Polym. 15 (1) (2003) 3–45.
[5] J.E. Szulejko, P. Kumar, A. Deep, K.-H. Kim, Global warming projections to 2100 using simple CO2 greenhouse gas modeling and comments on CO2 climate sensitivity factor, Atmospheric Pollution Res. 8 (1) (2017) 136–140.
[6] M.Z. Jacobson, Review of solutions to global warming, air pollution, and energy security, Energy Environ. Sci. 2 (2) (2009) 148–173.
[7] J. Ma, N. Sun, X. Zhang, N. Zhao, F. Xiao, W. Wei, Y. Sun, A short review of catalysis for CO2 conversion, Catal. Today 148 (3) (2009) 221–231.
[8] M.N. Khan, Y. van Ingen, T. Boruah, A. McLauchlan, T. Wirth, R.L. Melen, Advances in CO2 activation by frustrated Lewis pairs: from stoichiometric to catalytic reactions, Chem. Sci. 14 (47) (2023) 13661–13695.
[9] J. Wencel-Delord, T. Dröge, F. Liu, F. Glorius, Towards mild metal-catalyzed C–H bond activation, Chem. Soc. Rev. 40 (9) (2011) 4740–4761.
[10] C. Jia, T. Kitamura, Y. Fujiwara, Catalytic functionalization of arenes and alkanes via C−H bond activation, Acc. Chem. Res. 34 (8) (2001) 633–639.
[11] B.W.J. Chen, L. Xu, M. Mavrikakis, Computational methods in heterogeneous catalysis, Chem. Rev. 121 (2) (2021) 1007–1048.
[12] J.K. Nørskov, T. Bligaard, J. Rossmeisl, C.H. Christensen, Towards the computational design of solid catalysts, Nat. Chem. 1 (1) (2009) 37–46.
[13] C. Mukarakate, J.D. McBrayer, T.J. Evans, S. Budhi, D.J. Robichaud, K. Iisa, J. ten Dam, M.J. Watson, R.M. Baldwin, M.R. Nimlos, Catalytic fast pyrolysis of biomass: the reactions of water and aromatic intermediates produces phenols, Green Chem. 17 (8) (2015) 4217–4227.
[14] C. Amen-Chen, H. Pakdel, C. Roy, Production of monomeric phenols by thermochemical conversion of biomass: a review, Bioresour. Technol. 79 (3) (2001) 277–299.
[15] Suerbaev, K. A.; Aldabergenov, M. K.; Kudaibergenov, N. Z., Carboxylation of phenol and its derivatives with sodium ethyl carbonate. 2017, 6 (6), 543-547.
[16] J. Luo, S. Preciado, P. Xie, I. Larrosa, Carboxylation of phenols with CO2 at atmospheric pressure, Chem. – A Eur. J. 22 (20) (2016) 6798–6802.
[17] P.H. Pandey, H.S. Pawar, Cu dispersed ZrO2 catalyst mediated Kolbe- Schmitt carboxylation reaction to 4-hydroxybenzoic acid, Molecul. Catal. 530 (2022) 112595.
[18] A.S. Lindsey, H. Jeskey, The kolbe-schmitt reaction, Chem. Rev. 57 (4) (1957) 583–620.
[19] Economy, J.; Parkar, Z., High-temperature aromatic polyesters of p-hydroxybenzoic acid and their copolyesters. In *100+ Years of Plastics. Leo*

Baekeland and Beyond, Strom, E. T.; Rasmussen, S. C., Eds. American Chemical Society: 2011; Vol. 1080, pp 93-103.
[20] J.C. Védrine, Heterogeneous catalysis on metal oxides, Catalysts 7 (11) (2017) 341.
[21] R. Schlögl, Heterogeneous catalysis, Angew. Chem. Int. Ed. 54 (11) (2015) 3465–3520.
[22] H. Hattori, Heterogeneous basic catalysis, Chem. Rev. 95 (3) (1995) 537–558.
[23] O. Ohtaka, H. Fukui, T. Kunisada, T. Fujisawa, K. Funakoshi, W. Utsumi, T. Irifune, K. Kuroda, T. Kikegawa, Phase relations and equations of state of ZrO2 under high temperature and high pressure, Phys. Rev. B 63 (17) (2001) 174108.
[24] S. Zinatloo-Ajabshir, M. Salavati-Niasari, Facile route to synthesize zirconium dioxide (ZrO2) nanostructures: Structural, optical and photocatalytic studies, J. Mol. Liq. 216 (2016) 545–551.
[25] A. Bumajdad, A.A. Nazeer, F. Al Sagheer, S. Nahar, M.I. Zaki, Controlled synthesis of ZrO2 nanoparticles with tailored size, morphology and crystal phases via organic/inorganic hybrid films, Sci. Rep. 8 (1) (2018) 3695.
[26] J. Hafner, Ab-initio simulations of materials using VASP: Density-functional theory and beyond, J. Comput. Chem. 29 (13) (2008) 2044–2078.
[27] J.P. Perdew, K. Burke, M. Ernzerhof, Generalized gradient approximation made simple, Phys. Rev. Lett. 77 (18) (1996) 3865–3868.
[28] B. Himmetoglu, A. Floris, S. de Gironcoli, M. Cococcioni, Hubbard-corrected DFT energy functionals: The LDA+U description of correlated systems, Int. J. Quantum Chem. 114 (1) (2014) 14–49.
[29] H.J. Monkhorst, J.D. Pack, Special points for Brillouin-zone integrations, Phys. Rev. B 13 (12) (1976) 5188–5192.
[30] G. Kresse, J. Furthmüller, Efficiency of ab-initio total energy calculations for metals and semiconductors using a plane-wave basis set, Comput. Mater. Sci. 6 (1) (1996) 15–50.
[31] W. Tang, E. Sanville, G. Henkelman, A grid-based Bader analysis algorithm without lattice bias, J. Phys. Condens. Matter 21 (8) (2009) 084204.
[32] E. Sanville, S.D. Kenny, R. Smith, G. Henkelman, Improved grid-based algorithm for Bader charge allocation, J. Comput. Chem. 28 (5) (2007) 899–908.
[33] G. Henkelman, A. Arnaldsson, H. Jónsson, A fast and robust algorithm for Bader decomposition of charge density, Comput. Mater. Sci. 36 (3) (2006) 354–360.
[34] G. Henkelman, B.P. Uberuaga, H. Jónsson, A climbing image nudged elastic band method for finding saddle points and minimum energy paths, J. Chem. Phys. 113 (22) (2000) 9901–9904.
[35] G. Henkelman, H. Jónsson, Improved tangent estimate in the nudged elastic band method for finding minimum energy paths and saddle points, J. Chem. Phys. 113 (22) (2000) 9978–9985.
[36] A. Heyden, A.T. Bell, F.J. Keil, Efficient methods for finding transition states in chemical reactions: Comparison of improved dimer method and partitioned rational function optimization method, J. Chem. Phys. 123 (22) (2005) 224101.
[37] R. Ruh, T.J. Rockett, Proposed Phase Diagram for the System ZrO2, J. Am. Ceram. Soc. 53 (6) (1970) 360. -360.
[38] H. Fukui, M. Fujimoto, Y. Akahama, A. Sano-Furukawa, T. Hattori, Structure change of monoclinic ZrO2 baddeleyite involving softenings of bulk modulus and atom vibrations, Acta Crystallographica Section B-Structural Sci. Crystal Eng. Mater. 75 (2019) 742–749.
[39] P. Bouvier, E. Djurado, C. Ritter, A.J. Dianoux, G. Lucazeau, Low temperature phase transformation of nanocrystalline tetragonal ZrO2 by neutrons and Raman Scattering studies, Int. J. Inorg. Mater. 3 (7) (2001) 647–654.
[40] W. Piskorz, J. Gryboś, F. Zasada, P. Zapała, S. Cristol, J.-F. Paul, Z. Sojka, Periodic DFT study of the tetragonal ZrO2 nanocrystals: equilibrium morphology modeling and atomistic surface hydration thermodynamics, J. Phys. Chem. C 116 (36) (2012) 19307–19320.
[41] J.M. Liu, T. Wang, W.H. Jiang, G. Feng, L.F. Miao, T. Chen, Q. Wu, S.H. Wang, Preparation, characterization and formation mechanism of single-crystal zirconia micro-sheets, in: Processing and Application of Ceramics 13, 2019, pp. 229–234.
[42] B. Baldassarri, J. He, A. Gopakumar, S. Griesemer, A.J.A. Salgado-Casanova, T.-C. Liu, S.B. Torrisi, C. Wolverton, Oxygen vacancy formation energy in metal oxides: high-throughput computational studies and machine-learning predictions, Chem. Mater. 35 (24) (2023) 10619–10634.
[43] R.J. Baxter, P. Hu, Insight into why the Langmuir–Hinshelwood mechanism is generally preferred, J. Chem. Phys. 116 (11) (2002) 4379–4381.
[44] R. Prins, Eley–rideal, the other mechanism, Top. Catal. 61 (9) (2018) 714–721.
[45] R. Molavi, R. Safaiee, M.H. Sheikhi, N. Hassani, Theoretical perspective on CO oxidation over small cobalt oxide clusters, Chem. Phys. Lett. 767 (2021) 138361.
[46] Y. Zhao, H. Wang, J. Han, X. Zhu, D. Mei, Q. Ge, Simultaneous activation of CH4 and CO2 for Concerted C–C Coupling at Oxide–Oxide Interfaces, ACS Catalysis 9 (4) (2019) 3187–3197.
[47] P. Bouvier, E. Djurado, G. Lucazeau, T. Le Bihan, High-pressure structural evolution of undoped tetragonal nanocrystalline zirconia, Phys. Rev. B 62 (13) (2000) 8731–8737.